Measurement of the interactions between two ordering surfaces under symmetric and asymmetric boundary conditions

P. Richetti,[1] L. Moreau,[1] P. Barois,[1] and P. Kékicheff[2]
[1]*Centre de Recherche Paul Pascal, Centre National de la Recherche Scientifique, Avenue A. Schweitzer, 33600 Pessac, France*
[2]*Institut Charles Sadron, Centre National de la Recherche Scientifique, 6 rue Boussingault, 67083 Strasbourg, France*
(Received 2 January 1996)

With a surface forces apparatus we have measured the interaction between two surfaces immersed in the isotropic and the nematic phases of a lyotropic solution near its lamellar phase. A smectic ordering shows up near walls, giving a specific oscillatory force profile that is shown to be the sum of two contributions. The oscillations are the elastic response of the stack mechanically constrained by the confinement. The shape of the base line supporting the oscillations derives from the distribution of the smectic ordering between the two walls. In the case of fixed symmetric boundary conditions, the background is always attractive. However, under fixed asymmetric boundary conditions, the background turns out to be repulsive at short separations and becomes even repulsive at every separation when one of the two surfaces does not induce any order. [S1063-651X(96)08707-7]

PACS number(s): 68.15.+e, 64.70.Md, 68.45.Da

I. INTRODUCTION

Since the pioneering work of Sheng [1] concerning the effect of surface confinement on molecular ordering, many studies have probed the spatial dependence of the order parameter, especially for liquid crystals in contact with surfaces [2–6]. Much attention has also been devoted to phase transitions of confined liquid crystals [1,7,8] showing a strong dependence on surface anchoring [9,10], the geometry of enclosure [9,11–13], and the order of the transition [10].

Specific interactions between two ordering surfaces confining liquid-crystal molecules have been studied theoretically [7,14]. Such interactions were recently provided in the case of a second-order phase transition [15]. In addition, force measurements near a first-order phase transition have also been reported [16,17]. The present work completes our previous work [15] about interactions near a second-order phase transition, as it provides an extended theoretical background in the case of asymmetric boundary conditions, illustrated with further experimental investigations under these limits. A local smectic order is still considered, experimentally inquired with a lamellar lyotropic solution. The system studied is then a solution confined between two surfaces in equilibrium with a reservoir maintained above the smectic to nematic transition temperature so that the sample is not yet in the smectic phase in the bulk. The two walls interact with the fluid via an ordering potential, leading to a layering or a smectic positional order. In our experiment, the two surfaces of the surface forces apparatus (SFA) induced locally a layering of the disklike micelles. When the bulk phase transition is second order the thickness of the preordered films (presmectic film) wetting the walls grows continuously and diverges at the smectic transition. Now, when the two presmectic films wetting each wall overlap, the surfaces interact. The range of this specific interaction is given by the penetration length of the induced order. The shape of the interaction profile depends strongly on the boundary conditions or anchoring conditions on each surface, as we will show later.

In the present article, we report the experimental characterization of such pretransitional interactions both under symmetric and asymmetric boundary conditions. The former occurs when the two surfaces are strictly similar, whereas the latter is achieved when the two surfaces affect differently the positional ordering. To realize this situation experimentally, one of the two mica surfaces of the SFA has been coated with a polyelectrolyte in order to increase its roughness and then to reduce locally the smectic order in the wetting film.

The paper is organized as follows. First, in Sec. II we describe the force profiles obtained with a SFA near a second-order lamellar phase transition. In Sec. III we reconsider a very simple mean-field model (Landau-like) developed by de Gennes [14], choosing different boundary limits more suited to our experimental conditions. In Sec. IV we compare the modeling forces with our measurements. Finally, Sec. V is devoted to concluding remarks. We now present our experimental results.

II. EXPERIMENT

Using the SFA [18,19], we have investigated a binary aqueous lyotropic solution near its lamellar phase. This instrument is capable of measuring the separation between two mica surfaces immersed in a solution with an accuracy of ± 0.1–0.2 nm and the force within a sensitivity of 10^{-7} N. The molecularly smooth sheets of freshly cleaved mica are glued to cylindrical lenses of perpendicular axes and radius of curvature about 2 cm. The temperature in the enclosure surrounding the SFA was controlled to ± 0.02 °C, but stability was better in the SFA due to its large mass and thermal inertia. Although the temperature between the mica surfaces was not probed during the experiments, previous evaluations have shown a constant offset of 0.2 °C–0.4 °C compared to the outside temperature (T). Hereafter, the temperature difference between the outside and the bulk lamellar transition $\Delta T = T - T_{L_\alpha}$, which will be slightly overestimated, is chosen as the control parameter.

The lyotropic system was a mixture of water and an an-

ionic surfactant, cesium perfluoro-octanoate (CsPFO) [20]. The micelles formed above the critical micellization concentration are anisotropic with a disklike shape. At high micelle concentration, three distinct phases are found [20]: an isotropic phase (L_1) at high temperature, a smectic or a lamellar phase (L_α) at low temperature, and a nematic phase (N_D) for an intermediate range of temperature. At fixed composition, the N_D range is about 7 °C. Note that the L_1-N_D transition is weakly first order while the N_D-L_α transition is second order over most of the N_D composition range. To measure the presmectic interaction we have approached the lamellar phase from high temperatures, adjusting chemical compositions from one experiment to another so that the transitions were accessible around room temperature, i.e., between 18 °C and 31 °C, always above the Krafft temperature, which is about 13 °C at the studied concentrations. CsPFO was prepared by neutralizing an aqueous solution of pentadecafluorooctanoic acid (Aldrish Ltd.) with cesium hydroxide (Aldrish Ltd.). The neutralized solution was evaporated to dryness and the salt was recrystallized from isopropanol. The samples were prepared by weighing.

A. Interactions between two similar surface [15]

In this section we describe the force profiles obtained between two identical freshly cleaved micas, without any coating processing. Figure 1 shows the qualitative evolution of the profiles in the nematic and in the isotropic phases as ΔT is increased from the bulk nematic-lamellar transition. The curves of Fig. 1 display an oscillatory interaction with a period that is constant. Since one surface is suspended at the end of a spring of stiffness K, unstable regimes without data are seen when the force slope is greater than K [18]. Under these conditions, the system jumps from unstable to stable positions, leaving unexplored and inaccessible regions. An inward jump occurs from oscillation maxima upon compression of the surfaces (Fig. 1), while an outward jump occurs from the minima of the force profile upon separation (dilation). Every force profile presented in this figure and hereafter is drawn from several (generally three or more) inward (compression) and three outward (dilation) runs. The oscillations superimpose over an attractive background (defined as the envelope of the minima), while the maxima sit on a smooth decreasing function. Farther away from the smectic phase, a smaller number of oscillations are seen, concordant with a decreasing smectic correlation length. The oscillation amplitude decreases as ΔT is lowered. Likewise, the attractive background holding up the oscillations weakens progressively, as illustrated in Fig. 1.

Note that we have observed some scatter on the amplitudes for different samples of similar composition investigated at comparable ΔT. On the other hand, with the same sample, at fixed temperature, the scatter between successive measurements is remarkably low, even if different contact positions are probed.

In most of the N_d phase and in the L_1 phase the oscillatory presmectic forces are preceded by a weak attractive regime as illustrated, for instance, in Fig. 1(b) for separations between 40 and 80 nm or, in Fig. 1(c), for separations between 30 and 50 nm. Accordingly, the first oscillations that follow are often fully negative. On approaching the N_d-L_1 transition from the L_1 phase, the range of the attractive regime increases continuously. It reaches a maximum value at about 40 nm, close to the transition [Fig. 1(b)]. Below the transition, the strength of the attraction decreases progressively and disappears definitively about 3 °C or 4 °C beneath it, so that the first oscillations are equilibrated on both sides of the zero force line [Fig. 1(a)]. At short separations, the oscillations are on average more repulsive than attractive, whatever the temperature is. Figure 2 displays presmectic force profiles obtained just above the N_D-L_α transition showing a large number of oscillations [17 recorded in the profile of Fig. 2(b)]. The oscillation period was found to be 5.9 ± 0.1 nm, a value slightly lower than the smectic reticular distance for the same sample measured either with the SFA [15] or by small-angle x-ray scattering. The small decrease in the period from one phase to another is in agreement with structural measurements reported in the literature [21].

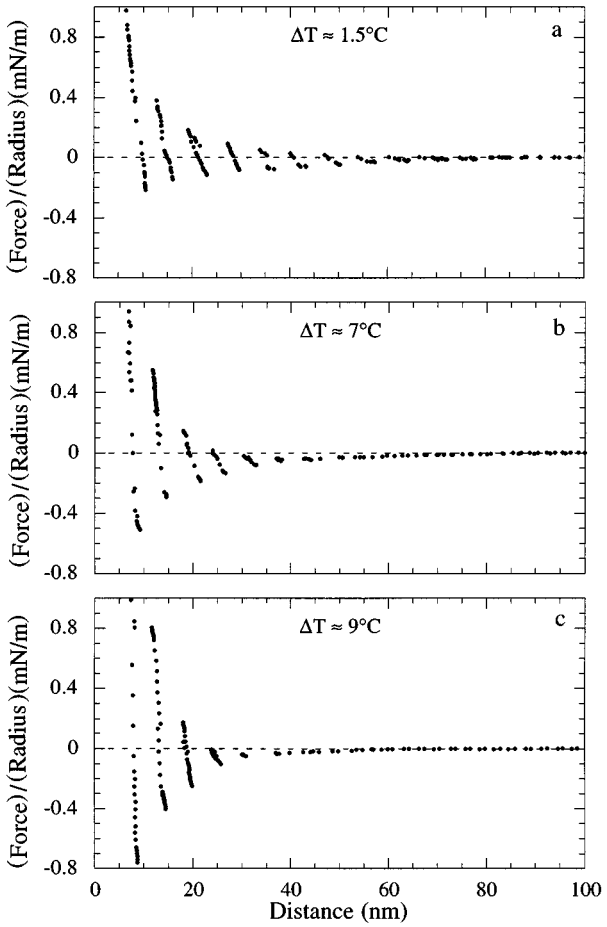

FIG. 1. Presmectic force profiles upon increasing the temperature between two bare micas immersed in a 34.3-wt. % CsPFO solution: (a) in the nematic phase, about 1.5 °C above the bulk lamellar transition (T_{L_α}); (b) close to the nematic-isotropic transition, about 7 °C above T_{L_α}; and (c) in the isotropic phase, about 9 °C above T_{L_α}. The oscillation background is attractive at all separation.

A comparison of the contact position at equilibrium in surfactant solution with that of bare micas indicates that a uniform surfactant bilayer (or micelles) is adsorbed on the two surfaces. This forms a hard wall (at about 6.2 nm) that can only be disrupted under high applied loads.

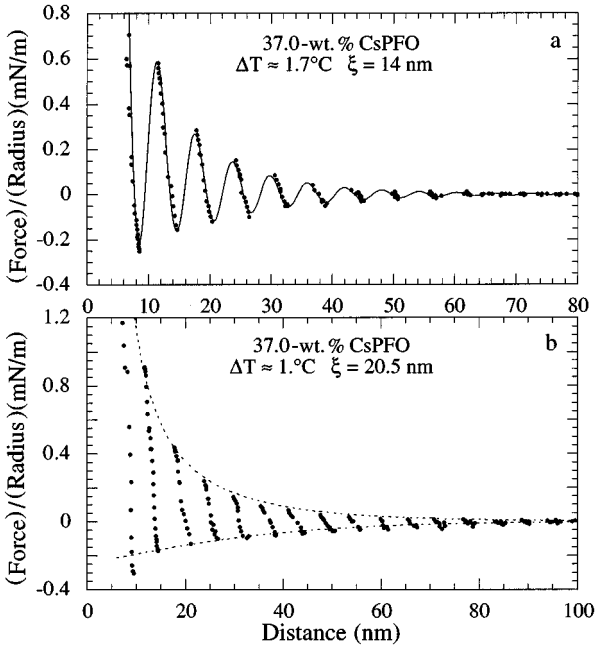

FIG. 2. Comparison between experimental force profiles (solid symbols) and the modeling force (41) for similar surfaces (bare mica). (a) In a 37-wt. % CsPFO solution, the line represents a fit giving ξ=14 nm and (b) in a 37.9-wt. % CsPFO solution, the dotted lines are best fits using $[\phi]$=0 and π, respectively, for the attractive background and the maximum envelope, giving ξ=20.5 nm.

B. Interactions between two dissimilar surfaces

In this section we describe the force profiles obtained between one bare mica and a mica treated by a coating process. One of the two mica surfaces has been covered with poly-*l*-lysine (Sigma Ltd.) from water outside the SFA. The following procedure was used to avoid any trace of bulk polyelectrolyte eventually mixed up with the liquid-crystal solution. First, two mica surfaces were glued down on the silica lenses of the SFA as usual [18] and contact was recorded in air. This defines the zero of separation. Then the upper mica, kept mounted on the piezoelectric tube, was removed carefully from the apparatus and immersed in 25-mg/l polymer solution. The incubation time was at least 4 h. As soon as the mica was removed from the polyelectrolyte solution, it was abundantly rinsed with fresh pure water, then dried by suction, and quickly set back into the SFA. The above procedure yields the same results as those reported in the literature [22], for which coating was performed in the SFA. Indeed, in a preliminary experiment, where the two micas were coated outside the SFA with the polypeptide, we have checked that the poly-*l*-lysine adsorbed in a flat configuration, as the negatively charged mica surfaces are neutralized. Accordingly, the net charge density is positive but remains quite small, even with the largest polymers.

Five different molecular weights (MW) of polymer have been tested. No qualitative difference with the symmetric case has been noted with the 4000- and 8000-MW polyelectrolytes. The force profiles are still oscillatory with an attractive minima envelope. The oscillation magnitudes appear slightly weaker, but remain almost within the scatter measured under symmetric boundary conditions. On the other hand, with the largest polyelectrolyte (140 000 MW), the force profiles are drastically modified. The oscillations are smeared out and replaced by a purely continuous repulsive interaction. Note that some difficulties were encountered to measure a profile that is reproducible even at different contact positions during the same experiment. Since the range and the strength of the interaction were found to vary by more than a factor of 2, these poorly reproducible force profiles are not shown here.

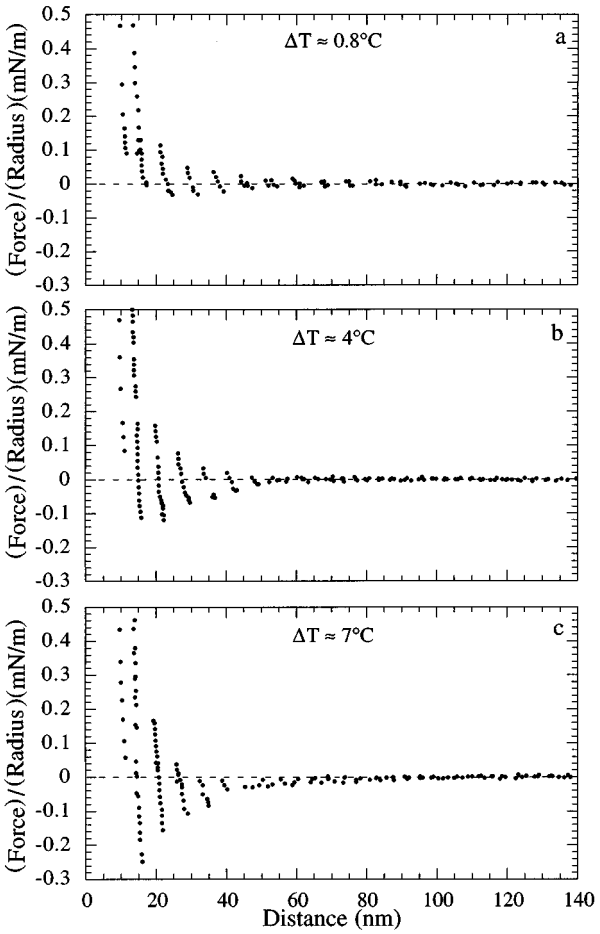

FIG. 3. Presmectic force profiles upon increasing the temperature between a bare mica and a mica coated with 25 000-MW poly-*l*-lysine immersed in a 38-wt. % CsPFO solution: (a) in the nematic phase, about 0.8 °C above the bulk lamellar transition (T_{L_α}); (b) still in the nematic phase, about 4 °C above T_{L_α}; and (c) close to the nematic isotropic transition, about 7 °C above T_{L_α}. The oscillation background turns out to be repulsive at short separations. The crossover moves back to larger separation as the lamellar transition is approached.

With intermediate molecular weights, namely, 25 000 and 44 000, a reproducible change on the force profile is found (Figs. 3 and 4). The main properties of the previous presmectic force profiles are recovered. Figure 3 displays the evolution of force profiles on approaching the lamellar transition between a bare mica and a coated mica with 25 000-MW poly-*l*-lysine. The profiles are still oscillatory; likewise the period of the oscillations is constant, the amplitudes decrease as separation increases, and the number of oscillations increases at the onset of the transition. The difference lies in

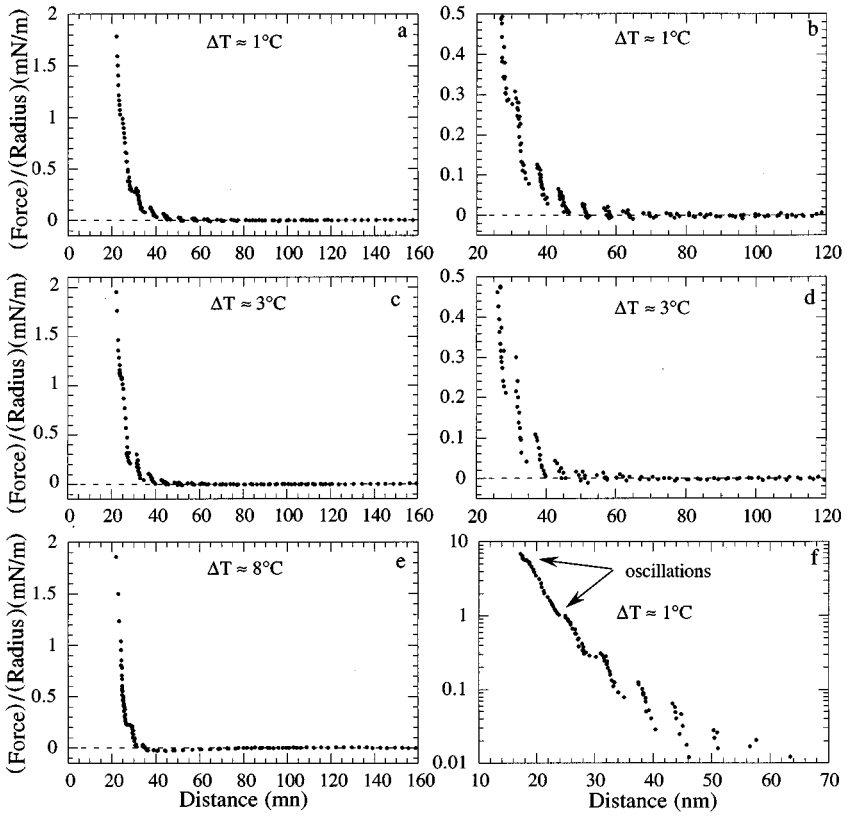

FIG. 4. Presmectic force profiles upon increasing the temperature between a bare mica and a mica coated with 44 000-MW poly-*l*-lysine immersed in a 38-wt. % CsPFO solution: (a) in the nematic phase, about 1 °C above the bulk lamellar transition (T_{L_α}); (b) an enlargement of the preceding plot; (c) still in the nematic phase, about 3 °C above T_{L_α}; (d) an enlargement of the preceding plot; (e) in the isotropic phase, about 7 °C above T_{L_α}; and (f) semilogarithmic scale for the first profile at 1 °C above T_{L_α} to evidence the largest oscillations. The oscillation background is almost always repulsive.

the background supporting the oscillations: still attractive at large separations, it turns out to be repulsive at shorter distances. The number of oscillations superimposed on the repulsive part of the background increases as ΔT decreases. This number grows from 1 for $\Delta T = 7$ °C [Fig. 3(c)] to 3 for $\Delta T = 0.8$ °C [Fig. 3(a)]. These two trends are fairly reproducible, as illustrated in Fig. 5, in which we compare the profiles obtained for another experiment, at two different contact positions. Some scatter on the amplitude of the oscillations is observed, slightly larger than under symmetric limits, except for the minimum height of the first oscillation before the contact (Fig. 5).

The features of the oscillation base line are confirmed when one of the two surfaces is treated with a longer polymer. Figure 4 displays the characteristic force profiles between a bare mica and a mica coated with 44 000-MW poly-*l*-lysine. Clearly evidence of an attractive background becomes more and more difficult. Most of the oscillations lie down on a repulsive background, within experimental accuracy, even at the highest temperatures [see the enlargements Figs. 4(b) and 4(d)]. The background is so repulsive that the first two oscillations close to contact become hardly visible. A logarithmic scale is then more appropriate to evidence them [Fig. 4(f)].

Finally, we note that the asymmetry of the boundaries has also some consequence on the amplitudes of the oscillations: the longer the polymers adsorbed on one surface the smaller the oscillation amplitudes [compare Figs. 2(b), 3, 5, and 4

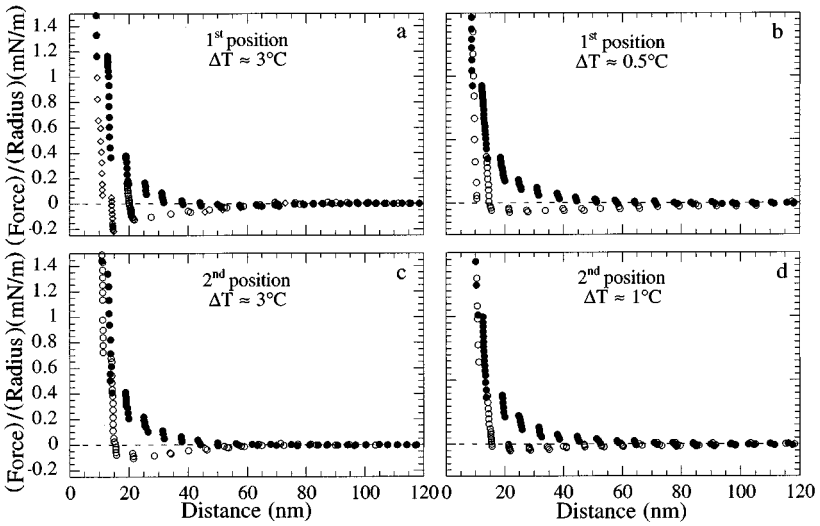

FIG. 5. Comparison of presmectic force profiles between a bare mica and a mica coated with 25 000-MW poly-*l*-lysine immersed in a 38-wt. % CsPFO solution obtained at two different contact positions. Solid symbols correspond to the force on approaching the surfaces, while the open symbols are the data obtained on separation starting only from the first oscillations close to contact. The first position is (a) about 3 °C above the bulk lamellar transition (T_{L_α}) and (b) about 0.5 °C above T_{L_α}. The second position is (c) about 3 °C above the bulk lamellar transition (T_{L_α}) and (d) about 1 °C above T_{L_α}.

corresponding to similar compositions and ΔT]. This last remark is consistent with the results (not shown) obtained when the coating is performed with the 140 000-MW poly-*l*-lysine.

In conclusion, the force profile recorded near the second-order lamellar phase transition is a damped oscillatory function. The oscillations are quite periodic and the number of oscillations increases on approaching the transition. The boundary conditions define the shape of the oscillation background. Under symmetric limits, the base line is always attractive, whereas it becomes repulsive at shorter separations under asymmetric boundary conditions. In the following section, a mean-field model is presented to account for these observations.

III. THEORETICAL BACKGROUND

The oscillations in the experimental force profiles suggest strongly that a positional ordering is induced by the surfaces with a layering of the discoid micelles, parallel to the surfaces. Two facts are in agreement with this interpretation. First, the period of the oscillations is very close to the reticular distance of the neighboring lamellar phase. Second, the number of oscillations, related to the number of layers (the penetration length), diverge at the onset of the transition like the smectic correlation length. The interaction between two parallel walls generating a smectic layering parallel to the surfaces while the bulk phase is not yet smectic (presmectic film) has been addressed by de Gennes [14]. To account for our data, we will follow the same approach.

A. Mean-field model

A natural approach is to describe the induced ordering in terms of a Landau order parameter and to approximate the interaction potential using a mean-field free energy. The order parameter describing the presmectic film is chosen to be the usual complex one-dimensional density wave $\Psi=\psi e^{i\phi}$. ψ measures the amplitude of the smectic density modulation, while the phase $\phi(x)$ is related to the layer displacement $u(x)$ by $\phi(x)=2\pi u(x)/a_0$, a_0 being the equilibrium smectic layer thickness. The phase $\phi(x)$ describes the local elastic deformation arising for most separations between the walls d, when d is not an integral multiple of the smectic layer thickness $d\neq na_0$. In this usual state, the presmectic film undergoes then an applied strain. In mean-field theory, the excess free energy owing to two parallel plates generating layered ordering may be written as a Landau expansion of the smectic order parameter in the vicinity of a second-order smectic phase transition [14]

$$f=\int_{-d/2}^{d/2}dx\left[\frac{\alpha}{2}\Psi^2+\frac{\beta}{4}\Psi^4+\cdots+\frac{L}{2}\left(\frac{d\Psi}{dx}\right)^2+\frac{K}{4}\left(\frac{d^2\Psi}{dx^2}\right)^2+\cdots\right]. \tag{1}$$

Following de Gennes, only the quadratic terms will be retained to capture the main trends. Since in bulk the sample is not yet in a smectic phase, α is positive in (1). $\xi=(L/\alpha)^{1/2}$ is defined as the smectic correlation length. After splitting the gradient term in two parts, the free energy is written as [14]

$$f=\frac{\alpha}{2}\int_{-d/2}^{d/2}dx\left[\psi^2+\xi^2\left(\frac{d\psi}{dx}\right)^2+\xi^2\psi^2\left(\frac{d\phi}{dx}\right)^2\right]. \tag{2}$$

The free energy is comprised of two contributions. The first two terms, depending only on the smectic density amplitude, account for the nonuniform distribution of the order between the two walls. This part is quite general, overtaking the smectic case studied here. It would be the interaction potential between two ordering walls for any system with a scalar order parameter far enough from a first-order transition. The third term in (2) is a coupling term, in which one may recognize the product of a strainlike term $d\phi/dx$ by a stresslike term $\alpha\xi^2\psi^2 d\phi/dx$. It is the elastic cost arising from the deformation imposed by the finite thickness of the confinement. Unlike the previous contribution, this second part of the free energy is intrinsic to the presmectic system.

First, the spatial distribution of the smectic density and the phase between the plates must be determined to calculate the interaction potential. Boundary conditions for both ψ and ϕ must also be defined. For the phase, following de Gennes [14], we will always assume that the smectic layers at both ends stick exactly to the wall. This imposes a phase difference

$$\phi(d/2)-\phi(-d/2)=\frac{2\pi}{a_0}(d-na_0)\equiv[\phi]. \tag{3}$$

For the amplitude, we assume that the walls impose constant values of the smectic densities at the surfaces, independent on the separation between them d,

$$\psi(-d/2)=\psi_1,\quad \psi(d/2)=\psi_2\quad \forall\ d. \tag{4}$$

This choice is laid down by the experimental system studied, where strong anchoring occurs on the walls. Indeed we have observed that a layer of surfactant is adsorbed on each surface and the thickness of this adsorbed layer fits with a bilayer or a monolayer of micelles. These adsorbed layers may be considered as the first ordered layers of the presmectic film at its both ends.

The profiles of the amplitude ψ and the phase ϕ are obtained by minimizing the free energy. Minimization with respect to the smectic amplitude ψ leads to the equation [14]

$$\psi\left[1+\xi^2\left(\frac{d\phi}{dx}\right)^2\right]=\xi^2\frac{d^2\psi}{dx^2}, \tag{5}$$

while minimization with respect to the phase ϕ leads to the expression [14]

$$\frac{d}{dx}\left(\psi^2\frac{d\phi}{dx}\right)=0, \tag{6}$$

which after integration becomes [14]

$$\frac{d\phi}{dx}=\frac{\Gamma}{\rho(x)}, \tag{7}$$

where Γ is a constant and $\rho(x)=\psi^2(x)$. As noted by de Gennes, since the strain (7) scales like ψ^{-2}, the distortion of layers would be not uniform along a constrained presmectic film. Between the two ordering walls, the smectic order is

expected to be more developed in the vicinity of the surfaces than at the center of the induced film, where ψ vanishes for large separations d. Accordingly, the elastic deformation is maximal in the soft central region and weaker near the surfaces where the smectic order is well established.

A presmectic film can be thought of as a series of springs, each having a different stiffness. The softer ones lie at the center and the stiffer ones are close to the walls. In comparison, a regular aligned smectic film (far enough to any transition) is a series of springs of identical stiffness, so the deformation through a smectic stack is uniform across the layers.

Using (6), Eq. (5) may then be rewritten as [14]

$$\psi+\frac{\Gamma^2\xi^2}{\psi^3}=\xi^2\frac{d^2\psi}{dx^2} \tag{8}$$

and has the first integral [14]

$$\psi^2-\frac{\Gamma^2\xi^2}{\psi^2}+C=\xi^2\left(\frac{d\psi}{dx}\right)^2, \tag{9}$$

where C is an integration constant, which we will define as [14]

$$C=\frac{1}{\rho_m}(\xi^2\Gamma^2-\rho_m^2) \tag{10}$$

with ρ_m the amplitude at the minimum of the profile x_m, where $d\rho/dx=0$. Note that the minimum would be located at the midpoint ($x_m=0$) only in the case of two similar surfaces, i.e., when symmetric boundary conditions are imposed. Multiplying both sides by ρ, Eq. (9) can be rewritten as [14]

$$(\rho-\rho_m)(\rho-\rho_m+2b)=\left(\frac{1}{2}\,\xi\,\frac{d\rho}{dx}\right)^2, \tag{11}$$

where b is related to the reduced stress Γ by [14]

$$b=\frac{1}{2\rho_m}(\xi^2\Gamma^2+\rho_m^2). \tag{12}$$

Equation (11) has a simple solution [14]

$$\rho=\rho_m+b\left[\cosh\left(2\frac{x-x_m}{\xi}\right)-1\right]. \tag{13}$$

Integrating the strain across the film allows us to obtain eventually the parameters b, x_m, and ρ_m. According to (7), the phase difference $[\phi]$ is given by [14]

$$[\phi]=\frac{2\pi}{a_0}(d-na_0)=\int_{-d/2}^{d/2}\frac{\Gamma}{\rho}\,dx, \tag{14}$$

the general solution of which is

$$[\phi]=\arctan\left[\left(\frac{2b-\rho_m}{\rho_m}\right)^{1/2}\tanh\left(\frac{d/2+x_m}{\xi}\right)\right]+\arctan\left[\left(\frac{2b-\rho_m}{\rho_m}\right)^{1/2}\tanh\left(\frac{d/2-x_m}{\xi}\right)\right]. \tag{15}$$

Before determining the profiles for the amplitude and the phase under different boundary conditions, let us complete the calculation of the interaction potential between the two ordering plates.

Using the Euler-Lagrange equation (5), it is straightforward to rewrite the free energy (2) as

$$f=\frac{\alpha}{2}\,\xi^2\left[\psi\,\frac{d\psi}{dx}\right]_{-d/2}^{d/2}=\frac{\alpha}{4}\,\xi^2\left[\frac{d\rho}{dx}\right]_{-d/2}^{d/2} \tag{16}$$

and Eq. (13) leads to

$$f=\frac{\alpha}{2}\,\xi b\left(\sinh\frac{d+2x_m}{\xi}+\sinh\frac{d-2x_m}{\xi}\right). \tag{17}$$

Let us examine first the case with two similar surfaces.

B. Fixed and symmetric boundary conditions

One considers here the case of two similar surfaces, inducing a smectic order. The boundary conditions imposed by the walls are identical (symmetric) and fixed regardless of the wall separation. The model developed above applies with the symmetric conditions

$$\psi_1=\psi_2=\psi_0,\quad \rho_1=\rho_2=\rho_0. \tag{18}$$

In other words, we have assumed a contact potential (zero range) between the surfaces and the liquid-crystal particles. By symmetry $d\rho/dx=0$ at the midpoint so that $x_m=0$. The phase difference (15) reduces to a simple expression

$$\tan^2\left(\frac{[\phi]}{2}\right)=\frac{2b-\rho_m}{\rho_m}\tanh^2\left(\frac{d}{2\xi}\right). \tag{19}$$

From (19), ρ_m and b are extracted by using Eq. (13) at the surfaces

$$\rho_0=\rho_m+2b\,\sinh^2\left(\frac{d}{2\xi}\right) \tag{20}$$

so that the smectic density at the midpoint is

$$\rho_m=\rho_0\,\frac{1+\cos([\phi])}{2\cosh^2\left(\frac{d}{2\xi}\right)}, \tag{21}$$

while the integration constant b is

$$b=\frac{1}{2}\,\rho_0\left(\frac{\cos^2\left(\frac{[\phi]}{2}\right)}{\cosh^2\left(\frac{d}{2\xi}\right)}+\frac{\sin^2\left(\frac{[\phi]}{2}\right)}{\sinh^2\left(\frac{d}{2\xi}\right)}\right). \tag{22}$$

Under these fixed and symmetric boundary conditions, we find amplitude and phase profiles similar in shape to those derived by de Gennes in [14]. The amplitude profile is obtained by combining (21) and (22) with (13). The smectic density modulation $\psi(x)$ decreases exponentially from the ordering surfaces to the midplane with the decay length ξ. The phase profile obtained by combining (21) and (22) with (19) is still an asymmetric function [see (19)]. When the

separation between the walls d is not an integral multiple of the smectic layer thickness a_0, $d \neq n a_0$, the distortion is mainly undergone by the central layers (around $x_m = 0$), where the smectic order is poorly established.

As pointed out by de Gennes [14], we note that when $[\phi]$ increases from 0 to π, the smectic density at x_m (21), at the middle of the presmectic film, drops off from $2b$ to 0. At zero stress, ρ_m takes a maximal value of $2b$, but after a compression or a stretching by half a layer this density falls off to zero; the local smectic order is lost in the center of the gap. This melting mechanism allows the presmectic film to release the stress undergone in adjusting the number of layers in the stack from n to $n \pm 1$. The relaxation mechanism in a regular smectic film is very different. Indeed, edge dislocation loop nucleations or annihilations are expected to release the stress and to adjust the number of layers in the confinement [23,24].

Combining (22) and (17) and after some arrangements, the interaction potential between two similar surfaces inducing smectic ordering under fixed and symmetric boundary conditions takes the form [15]

$$f = \alpha \xi \rho_0 \left(\tanh \frac{d}{2\xi} + \frac{1 - \cos([\phi])}{\sinh(d/\xi)} \right). \tag{23}$$

We find again the two contributions underlined previously in (17). The first term, which is very general and phase independent, is the attractive amplitude contribution arising from the symmetric nonuniform distribution of a scalar order parameter as calculated by various authors for different physical entities [7,25]. The second term is the elastic contribution of the constrained system, a damped oscillatory function of period a_0. Unlike the first term, this contribution is phase dependent and specific to the smectic order. In summary, the symmetric distribution of the smectic order between the walls leads to an attractive background upon which oscillations arising from the elastic response of the distorted layers are superimposed.

In the asymptotic regime, when $d \gg \xi$, both the attractive background

$$f_{[\phi]=0} = \alpha \xi \rho_0 \tanh(d/2\xi) \tag{24}$$

and the maximum envelope

$$f_{[\phi]=\pi} = \alpha \xi \rho_0 \coth(d/2\xi) \tag{25}$$

follow an exponential law with a decay length ξ. This interaction potential between two plates is short range as long as the system is not too close to a second-order phase transition. In this close vicinity, higher-order terms ($\Psi^4, \Psi^6, \ldots$) as well as thermal fluctuations can no longer be neglected in the free energy (1).

In comparison, for a regular smectic sample confined under a homeotropic alignment, the interaction profile is a long-range oscillatory curve [15,26]. The distance between two successive minima must be equal to $b a_0$ [26], where b is the Burgers vector of the edge dislocation loop, allowing the system to release the elastic stress by adjusting the number of layers from n to $n \pm b$ when the applied strain is $d \approx (n \pm b/2) a_0$ [23,24,26]. The parabolic oscillations lie on a zero background as long as the surfaces do not enhance locally the bulk order parameter [15,26].

In de Gennes's model [14], the ordering interaction between the walls and the anisotropic fluid is also assumed to be a contact potential, expressed now by a linear coupling term between the order parameter and a conjugate field $-h_s[\Psi(-d/2) + \Psi(d/2)]$. In fact, this surface potential fixes the amplitude slope of the order parameter profile at the surfaces and not the amplitudes as before, whatever the separation between the walls $\nabla_x \psi(-d/2) = -\nabla_x \psi(d/2)$. Under these self-consistent boundary conditions, the free energy can be again solved exactly and has the expression

$$f = -\frac{h_s^2}{\alpha \xi} \coth \frac{d}{2\xi} \left(1 - \frac{1 - \cos([\phi])}{\cosh(d/\xi) - \cos([\phi])} \right). \tag{26}$$

These self-consistent conditions might be more relevant for weak anchoring, while the other limit is better suited for stronger anchoring.

C. Fixed and asymmetric boundary conditions

The case of two dissimilar surfaces, inducing the smectic order with different strength, is now considered. As previously, we assume that these strengths are constant whatever the separation d, defining fixed and asymmetric boundary conditions

$$\psi_1 \neq \psi_2, \quad \rho_1 \neq \rho_2. \tag{27}$$

Arbitrarily we choose $\psi_1 > \psi_2$ [$\psi(-d/2) = \psi_1$]. Under these limit conditions x_m is no longer located at the midpoint of the presmectic film, but somewhere between 0 and $d/2$ and even beyond $d/2$ for certain conditions, as will be shown later,

$$x_m = \frac{d}{2} - \frac{\xi}{2} \operatorname{arcosh}\left(1 + \frac{\rho_1 - \rho_m}{b} \right). \tag{28}$$

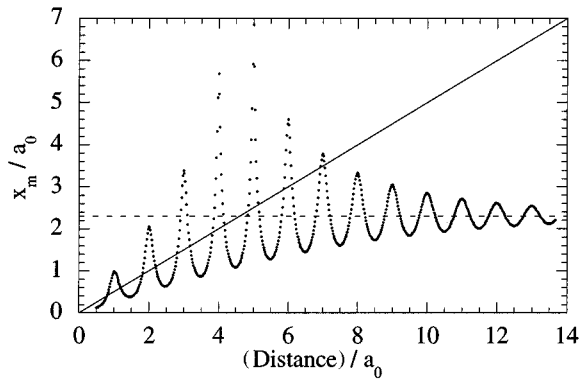

FIG. 6. Theoretical position of the minimum x_m, in the order parameter amplitude profile between two dissimilar ordering surfaces as a function of their separation [Eq. (33) with $\Delta\rho = 0.45$ and $\xi/a_0 = 4$]. The diagonal line is the position of the confinement boundary $x(d/2)$. When x_m is beneath the diagonal, x_m stands then inside the confinement, whereas x_m becomes a virtual point outside of the confinement when x_m goes above the diagonal. The dotted line is the asymptotic limit [Eq. (34)] at large separation. Note that the minima corresponding to $[\phi] = \pi$ lie always inside the confinement.

Let us define two parameters $\overline{\rho}=(\rho_1+\rho_2)/2$ and $\Delta\rho=(\rho_2-\rho_1)/2$. Equations (12) and (13) then take the expressions

$$b=\Delta\rho\,\frac{1}{\sinh(d/\xi)\sinh(2x_m/\xi)} \tag{29}$$

and

$$\rho_m=\overline{\rho}-\Delta\rho\,\frac{\cosh(d/\xi)\cosh(2x_m/\xi)-1}{\sinh(d/\xi)\sinh(2x_m/\xi)}. \tag{30}$$

Substituting b from (29) in (17), we get the interaction potential

$$f=\Delta\rho\alpha\xi\,\frac{1}{\tanh(2x_m/\xi)}. \tag{31}$$

x_m can be determined from Eqs. (29), (30), and (15). The latter can be rewritten as

$$\tan([\phi])=[\rho_m(2b-\rho_m)]^{1/2}\,\frac{\tanh[(d+2x_m)/2\xi]+\tanh[(d-2x_m)/2\xi]}{\rho_m+(2b-\rho_m)\tanh[(d+2x_m)/2\xi]\tanh[(d-2x_m)/2\xi]}. \tag{32}$$

Like in the symmetric case, when no strain is applied ($[\Phi]=0$), ρ_m takes a maximal value of $2b$ and falls off to 0 after a compression or a decompression of half a layer ($[\Phi]=\pi$). From (29), (30), and (32), one derives x_m, the minimum in the amplitude profile,

$$x_m=\frac{\xi}{2}\,\mathrm{arctanh}\left(\frac{\Delta\rho\,\sinh(d/\xi)}{\overline{\rho}\,\cosh(d/\xi)-(\rho_1\rho_2)^{1/2}\,\cos([\phi])}\right). \tag{33}$$

In Fig. 6 we give an example of x_m as a function of the separation between the two surfaces under asymmetric boundary conditions. We note that x_m may become a virtual point, overtaking the boundary of the confinement where the smectic density is the lowest. At large separations, when $d\gg\xi$, the amplitude profile between the two surfaces exhibits always the minimum x_m, like in the case of symmetric boundary conditions. In this asymptotic regime, x_m takes the value

$$d\gg\xi\Rightarrow x_m\to\frac{\xi}{2}\,\mathrm{arctanh}(\Delta\rho/\overline{\rho}). \tag{34}$$

On the other hand, at smaller separations, x_m may move out from the confinement, depending on the asymmetric ratio $\Delta\rho/\overline{\rho}$, the phase difference $[\phi]$, and the correlation length ξ, so that the amplitude profile between the two surfaces is a continuously decreasing function. However, under strain, the minimum always returns to the confinement, as we will now demonstrate. Let us consider the system under the maximum of applied strain when $[\phi]=\pi$. Since $0\leqslant\Delta\rho/\overline{\rho}\leqslant 1$, there exists an upper limit for $x_m^{\min}=x_m([\phi]=\pi)$ according to (33),

$$\tanh(2x_m^{\min}/\xi)\leqslant\frac{\sinh(d/\xi)}{\cosh(d/\xi)+[1-(\Delta\rho/\overline{\rho})^2]^{1/2}}\leqslant\tanh(d/\xi) \tag{35}$$

and, accordingly,

$$x_m^{\min}\leqslant\frac{d}{2}. \tag{36}$$

The melting mechanism to release the stress by changing the number of layers from n to $n\pm1$ remains physically possible since x_m transits from a virtual to a real status under strain.

Combining (31) and (33) and after some arrangements to separate the elastic contribution from the order distribution contribution, the interaction potential between two dissimilar surfaces inducing smectic ordering under fixed boundary conditions has the form

$$f=\alpha\xi(\rho_1\rho_2)^{1/2}\left(\frac{[1-(\Delta\rho/\overline{\rho})^2]^{-1/2}\,\cosh(d/\xi)-1}{\sinh(d/\xi)}+\frac{1-\cos([\phi])}{\sinh(d/\xi)}\right). \tag{37}$$

The second term is the elastic contribution of the constrained system, which is the same damped oscillatory function of period a_0 as for two similar surfaces (23). The first term is the amplitude contribution arising from the asymmetric nonuniform distribution of a scalar order parameter between the two surfaces. The amplitude contribution can be rewritten as

$$f_{[\phi]=0}=\frac{\alpha\xi}{\sinh(d/\xi)}\,[\overline{\rho}\,\cosh(d/\xi)-(\overline{\rho^2}-\Delta\rho^2)^{1/2}]. \tag{38}$$

It is easy to check that when $\Delta\rho$ vanishes, Eq. (38) tends to the symmetric solution (25). Let us calculate the corresponding force ($F=-\mathrm{d}f/\mathrm{d}d$) between the two dissimilar ordering plates

$$F_{[\phi]=0}=\frac{\alpha}{\sinh^2(d/\xi)}\,[\overline{\rho}-(\overline{\rho^2}-\Delta\rho^2)^{1/2}\,\cosh(d/\xi)]. \tag{39}$$

Two limit situations can be distinguished. Under symmetric conditions ($\Delta\rho=0$), the previously studied case, the force and the background of the free energy are always attractive. The second limit occurs under strong asymmetry, when one of the two surfaces does not induce any order at all; for instance, when $\rho_2=0$ and $\Delta\rho=\overline{\rho}$, the force and the background of the free energy are always repulsive. For interme-

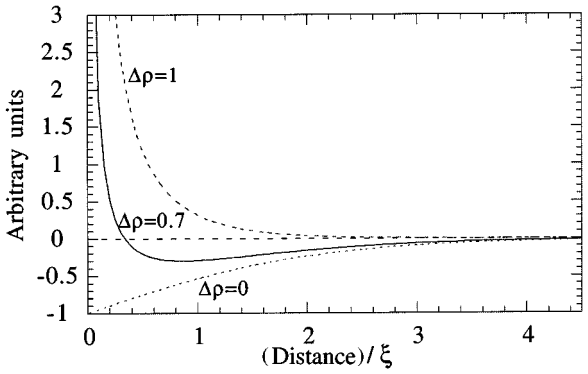

FIG. 7. Theoretical oscillation background under different fixed limit conditions. When the two ordering surfaces are similar $\Delta\rho=0$ the base line is always attractive, whereas the background becomes always repulsive when one of the two surfaces does not induce any order $\Delta\rho=1$. For intermediate asymmetric conditions, for instance, when $\Delta\rho=0.7$, the curve is attractive at large separations, but turns out to be repulsive at shorter separations.

diate asymmetric boundary conditions, the force remains attractive at large separations, but turns out to be repulsive at shorter separations. Accordingly, a minimum emerges along the oscillation background, as illustrated in Fig. 7, at the separation $d_{\min}$,

$$d_{\min}=\xi\ \mathrm{arcosh}[\overline{\rho}/(\rho_1\rho_2)^{1/2}], \tag{40}$$

scaling linearly with the smectic correlation length; the closer the smectic transition the larger the separation where the change of regime occurs.

In summary, the transition from a symmetric to an asymmetric distribution under fixed boundary conditions leads to a qualitative change of the interaction potential only for the ordering distribution contribution. The latter transits continuously from an attraction to a repulsion. On the other hand, the elastic contribution giving the oscillations in the force profiles remains the same in form and is only softened by the asymmetry. Indeed, since its strength depends on $(\rho_1\rho_2)^{1/2}$, the contribution and, accordingly, the oscillation amplitudes are maximal under symmetric conditions and vanish when one of the two surfaces does not induce any order.

IV. DISCUSSION

A comparison between our experimental results and the theory developed above is now performed. The surface geometry in the SFA is not that of two parallel plates, as discussed in Sec. III, but two crossed cylindrical surfaces [18]. For the current case, we can use the Derjaguin approximation [27] $F(d)=2\pi Rf(d)$ relating the force $F(d)$ between two identical crossed cylinders of radius R and the interaction potential $f(d)$ between two parallel plates when $d\ll R$ (here $R\approx 2$ cm). Indeed, the Derjaguin approximation is expected to hold for presmectic interactions because they fall off sufficiently rapidly [exponentially; see (24) and (25)] with distance and their range is much smaller than the experimental cylinder radii.

However, this approximation concerns only the presmectic interaction and may suffer from the effect of additional elastic deformations arising from the curved geometry. In considering homeotropic orientation as suggested by the periodic oscillatory force profiles, two other elastic distortions can be thought of: a global splay-bend deformation of the nematic director when the sample confined between the surfaces is in the nematic phase and a local bend distortion of the presmectic layers induced near the surfaces. The global strain has been already addressed by Horn, Israelachvili, and Perez [28] for the surface geometry of the SFA. The splay-bend elastic force between the two surfaces is not short ranged and may be estimated as [28]

$$F_{\mathrm{SB}}/R=2\pi\,\frac{K_{33}}{R}\ln(t_s/d), \tag{41}$$

where t_s is the thickness of the sample at the edge of the surfaces and K_{33} the bend elastic constant. Using typical experimental values $t_s=1$ mm, $R=2$ cm, and $K_{33}<10^{-11}$ N [29,30], the splay-bend elastic force is about 10^{-4} mN/m, i.e., 100 times smaller than the apparatus sensitivity at a separation of $d=10$ nm. Never would this specific curved geometry force compete with the presmectic interaction.

The magnitude of the elastic energy due to the bend of the presmectic layers covering each surfaces can be also estimated. Let us consider the presmectic films as regular smectic stacks of thickness ξ. The excess curvature energy may be then estimated as

$$\Delta E_c\approx\frac{K_c}{R^2}\,\xi, \tag{42}$$

where K_c is the layer bend elastic constant. A numerical application with $K_c<10^{-11}$ N gives a negligible value (10^{-11} mN/m) compared to the considered presmectic energy. In conclusion, the additional elastic deformations arising from the crossed-cylinder geometry of the surfaces are too weak to invalidate the Derjaguin approximation.

A. Interactions between two similar surfaces [15]

As mentioned earlier, the choice of fixed boundary conditions seems to be more suited to account for our data since a surfactant layer is adsorbed on each surface. This assumption may be justified as well by a qualitative comparison between the measured force profiles under symmetric limits (Fig. 1) and the modeling interaction potentials under fixed conditions (23) and self-consistent conditions (26). For the latter, the modeling potential (26) predicts that the interaction between the walls averaged over the oscillations is zero when $d\gg\xi$, but at short separations the averaged free energy becomes attractive. Now, in assuming a fixed smectic density on the surfaces, the modeling potential (23) predicts that the averaged interaction in the asymptotic regime is still neutral, but at short separations it turns out to be repulsive. From the presmectic curves of Figs. 1 and 2, on average, the measured forces are repulsive. A larger portion of the oscillations close to the contact stands above zero. In regard to this criterion, again fixed boundary conditions seem well suited for our experiment. However, far from the lamellar transition some oscillations may be negative.

As discussed previously in Sec. II, in most of the N_d phase and in the L_1 phase the oscillatory presmectic forces are preceded by a weak attractive regime; illustrations are

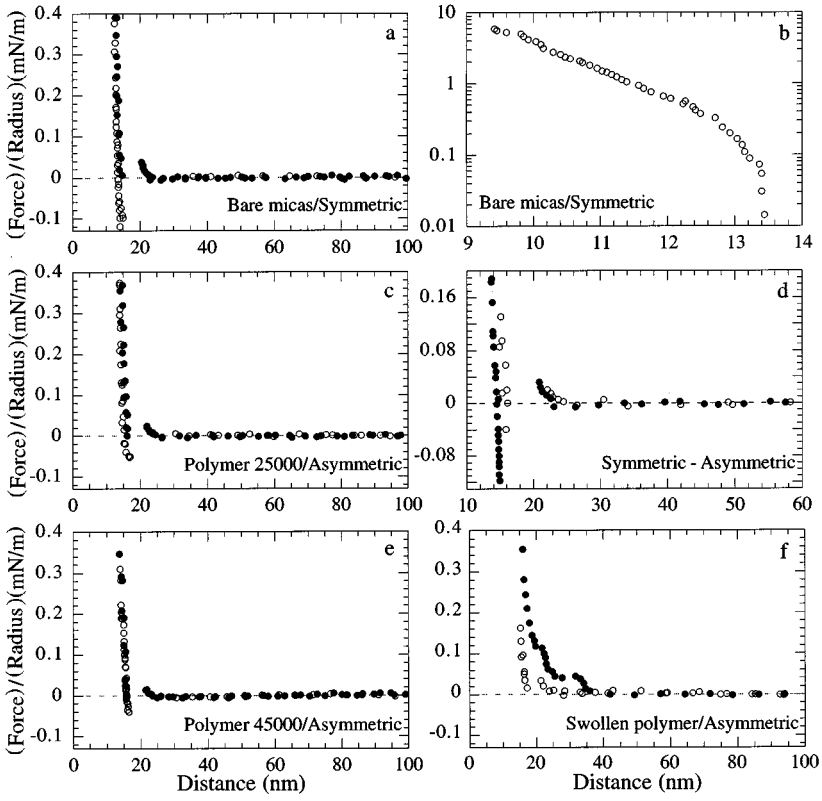

FIG. 8. Comparison of depletion force profiles between different pairs of micas immersed in a 6-wt. % CsPFO solution. Force profile between two bare micas: (a) large scale and (b) enlargement at short separations evidencing the deviation owing to the depletion from the exponential electrical double-layer repulsion. Force profiles between a bare mica and a mica coated with poly-*l*-lysine of (c) 25 000 MW and (e) 44 000 MW. (d) Direct comparison of two profiles: solid and open symbols correspond to the data of (a) and (e), respectively. (f) Unreproducible force profile between a bare mica and a mica coated with 44 000-MW poly-*l*-lysine adsorbed in an extended configuration from a salted solution (solid and open symbols were recorded on compression and on separation, respectively).

given in Fig. 1(b) for separations between 40 and 80 nm and in Fig. 1(c) for separations between 30 and 50 nm. Accordingly, the first oscillations that follow are often fully negative. On approaching the N_d-L_1 transition, the range of the attractive regime increases continuously. It reaches a maximum value close to the transition [Fig. 1(b)]. Below the transition, the strength of the attraction decreases progressively. A likely interpretation is that a prenematic film follows the presmectic film. Near the ordering walls there exists the presmectic film with both an orientational and a positional order. Recalling that both bulk transitions are either second order or weakly first order, we can suppose that while the positional order is lost outside the presmectic film, the orientational order is kept over a thicker layer giving a prenematic film. Its thickness depends on the distance from the N_d-L_1 transition. In this picture, an attraction is expected before the presmectic oscillatory force when the prenematic films of each surface begin to overlap. When the nematic order can be described by a scalar order parameter (uniaxial), the interaction between the two confining surfaces would be identical to the amplitude term of (23) giving the attractive background [7,25]. Even in the nematic phase the attraction would be effective as long as the nematic order parameter in the bulk is weaker than the value imposed at the interface of the presmectic and prenematic films.

This attractive regime disappears definitively about 3 °C or 4 °C beneath the N_d-L_1 transition, leaving then only about 3 °C down to the lamellar transition with pure presmectic profile. The temperature range over which numerical fits can be performed is then quite limited. Using the Derjaguin approximation [27], the model predicts the force for the experiment [15]

$$F=2\pi R\alpha\xi\rho_s\left(\tanh[(d-d_a)/2\xi]+\frac{1-\cos([\phi])}{\sinh[(d-d_a)/\xi_{\|}]}-1\right), \tag{43}$$

where d_a is the zero stress separation without any smectic layer owing to the adsorbed surfactant layers. The third term arises from the geometry integration, ensuring a zero force at large separations. In Fig. 2(b) we present the result of a numerical fit performed both on the background and the maximum envelope using (41) with $[\phi]=0$ and π, respectively. The modeling force is in remarkable agreement with the measured profile, except for the first minimum. The correlation length ξ extracted from the fit was 20.5 ± 1 nm, which is between two or three times the layer thickness. The same fit procedure has been carried out with the force curve of Fig. 2(a), in which we have plotted the full modeling force.

Unfortunately, our experimental device does not allow us to examine further the theory in testing, for instance, the predicted power law for the correlation length ξ with the temperature. As mentioned earlier, the exact value of temperature between the two surfaces is inaccessible.

B. Interactions between two dissimilar surfaces

Obviously, from a qualitative point of view, our force measurements between a coated mica and a bare mica are in good agreement with the asymmetric theoretical predictions. First, we have well verified that the oscillation magnitudes are softened when the asymmetry on the boundaries is enhanced. The largest amplitudes have been found under symmetric conditions, whereas the oscillations disappear when one surface is coated with the longest polymers. Second, the oscillation background is found to evolve from attractive to

repulsive as the asymmetry is enhanced. Finally, when a minimum is present in the oscillation background, its location evolves correctly with ΔT; the closer to the lamellar transition, the farther the minimum is from the contact, as exemplified in Fig. 3. The question of the nature of the force driving this behavior then arises. Is this behavior due to a difference in the strength to induce the smectic layering when a surface is treated with the poly-*l*-lysine or is it due to something else, for instance, an extra steric force owing to partially desorbed polymers? Such desorption of polymers has already been observed when surfactant is added to the solution [31].

To test such a possibility, the force profiles were measured in surfactant solution, at low concentration in micelle, 6 wt. %, before the emergence of the structural oscillations. The results are presented in Fig. 8. Between two bare micas [Figs. 8(a) and 8(b)] the recorded interaction has the usual appearance of the competition between a depletion profile and an electrical double-layer repulsion between two charged surfaces confining a micellar solution [32]. At this concentration only one weak oscillation, located at about 20 nm, arises from the confinement of a last layer of micelles. Then their depletion from the gap at smaller separations causes a deficit in osmotic pressure and leads to the minimum in the force profile around 14.5 nm [Fig. 8(a)]. On approaching the surfaces farther, a double-layer repulsion occurs between the charged adsorbed surfactant layers on each mica [Fig. 8(b)]. A direct comparison points out that the strength of the structural oscillation and the depletion is significantly reduced between two dissimilar surfaces. Figures 8(c) and 8(e) illustrate such an evolution when one surface is coated, respectively, with 25 000- and 44 000-MW poly-*l*-lysine. These force profiles show that the polyelectrolyte was adsorbed in flat configuration since no additional steric repulsion was observed. We found just a small shift in the locations [Fig. 8(d)] (about 1.0 nm), suggesting that the polymer, which may be slightly swollen, is inserted between the mica and an adsorbed layer of surfactant. This picture of two successive adsorbed layers is still consistent with fixed boundary conditions. In Fig. 8(f) we present for comparison the equivalent force profile obtained when one of the surfaces has been coated with the 44 000-MW polymer from a electrolyte solution ($[NaNO_3]=10^{-3}M$). In agreement with the literature [33,34], we found that the polypeptide is no longer adsorbed in a flat configuration but in an extended configuration. As the two surfaces are approached for the first time, a long-range repulsion is experienced from around 50 nm, resulting in a steric interaction. This first compression causes irreversible changes in the conformation of the adsorbed polymer layer. Indeed, a second approach gives a force profile different both in range and in magnitude. Reproducible force profiles can only be obtained after several successive compression-dilation cycles. Although the steric repulsion became shorter range (35 nm) and much weaker than during the first compression of the surfaces [Fig. 8(f)], it is still qualitatively different from the profiles displayed in Figs. 8(c) and 8(e). A second signature of adsorbed polymers in an extended configuration is the slow relaxation dynamics, especially upon the expulsion of the last layer of micelles out from the confinement. This feature is actually a quite efficient criterion to discriminate between the two adsorbed configurations. This complementary study shows that the adsorbed polymer remains preferentially in a flat configuration on the mica surface when immersed in a CsPFO solution (at least for the 25 000- and 44 000-MW macromolecules).

Using the Derjaguin approximation [27], the mean-field model predicts the following force between two dissimilar surfaces in a crossed cylindrical geometry:

$$F=2\pi R\alpha\xi\overline{\rho}\left(\frac{\cosh[(d-d_a)/\xi]}{\sinh[(d-d_a)/\xi]}-\sqrt{1-\Delta\rho^2/\overline{\rho}^2}\,\frac{\cos([\phi])}{\sinh[(d-d_a)/\xi]}-1\right). \tag{44}$$

As in (41), the third term arises from the geometry integration ensuring a zero force at large separation. Similarly d_a is still the zero stress separation without any smectic layer, corresponding to the adsorbed surfactant layer thickness on one of the two surfaces. In the symmetric case, this thickness was assumed to be equal on the two surfaces and found very close to the expected thickness of a bilayers of surfactants. Under asymmetric conditions, d_a measures the thickness of the adsorbed layer on the treated surface including both the polymer and the surfactant aggregates. Equation (42) is a five-independent-parameter modeling force. Two of them—a_0, the smectic thickness, and d_a—can be extracted easily from data by plotting the minimum locations of the force profile oscillations as a function of their rank [15]. Straight lines are found (not shown here). Their slopes give a_0 and the intercepts with the coordinate axis allow us to determine d_a for each experiment. The fit procedure on the force profiles consists then in determining the three remaining parameters: the prefactor of (42), $2\pi RL\overline{\rho}$, the smectic correlation length ξ, and the anisotropic ratio $\Delta\rho/\overline{\rho}$.

In Fig. 9 we present such numerical fits performed on two different experiments when one of the two mica surfaces was coated with the 25 000-MW polyelectrolyte. Although the agreement between the modeling force and the data is rather satisfying, on most of oscillations we have always met some difficulties for the first two oscillations close to the contact. These difficulties are more profound than the complication expected to arise when a continuum theory is applied for data obtained with only two presmectic layers. For instance, with the first experiment presented in Fig. 3 and analyzed in Figs. 9(a) and 9(b), we have observed some hysteresis during the measurement of the first two oscillations, the magnitude of which depends on the load applied over a compression run. During this experiment, we have never observed an inward jump from the second oscillation to the first one at the equilibrium separation of $1.5a_0$. The transition is rather continuous, the first oscillation being progressively attained by increasing the load. This behavior suggests that the squeezing of the surfactant micelles from the gap was somehow locked by the ill-ordered layer adsorbed on the treated mica. On the other hand, after the first oscillation was described upon a strong compression, an outward jump occurred on a decompression run. The location is not exactly at the expected separation of $1.a_0$ but lies at a slightly larger separation, as illustrated in Fig. 9. It seems likely that separation of the surfaces enables the surfactant micelles to be incorporated into the gap, as if the former strong compression had

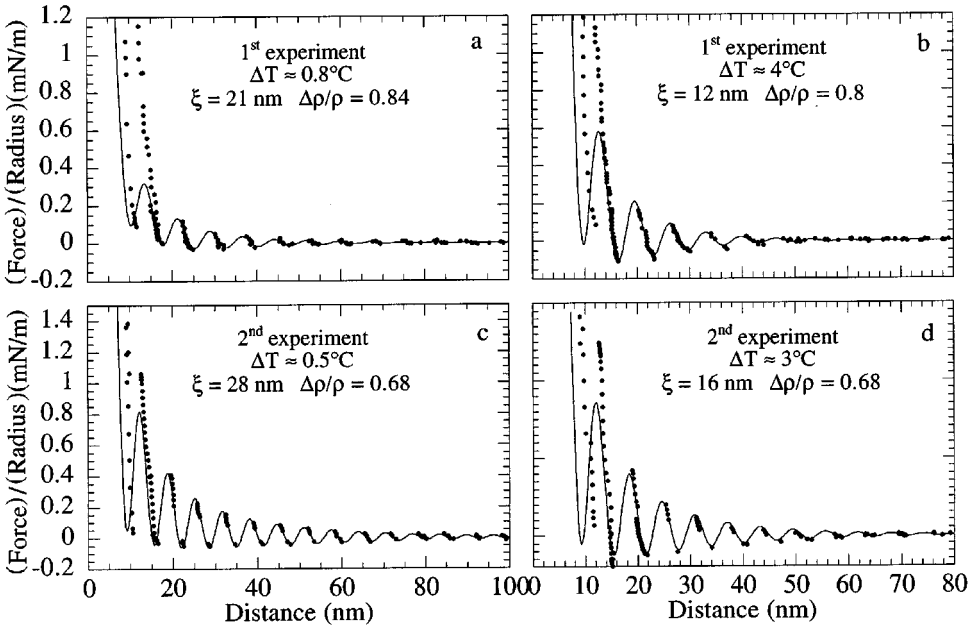

FIG. 9. Comparison between experimental force profiles and the modeling force (42) for two dissimilar surfaces. The solid symbols are the data measured between a bare mica and a mica coated with 25 000-MW poly-*l*-lysine immersed in a 38-wt. % CsPFO solution, while the lines represent the fit curves. Two similar experiments yielding slightly different results are presented. The first experiment is (a) near the lamellar transition, with a fit using a prefactor $2\pi RL\overline{\rho}=3.1\times10^{-9}$ mN, an asymmetric ratio $\Delta\rho/\overline{\rho}=0.84$, and a correlation length $\xi=21$ nm, and (b) at higher temperature with a fit using $2\pi RL\overline{\rho}=5.0\times10^{-9}$ mN, $\Delta\rho/\overline{\rho}=0.8$, and $\xi=12$ nm. The second experiment is (c) near the lamellar transition, with a fit using $2\pi RL\overline{\rho}=5.5\times10^{-9}$ mN, $\Delta\rho/\overline{\rho}=0.68$, and $\xi=28$ nm and (b) at higher temperature with a fit using $2\pi RL\overline{\rho}=6.4\times10^{-9}$ mN, $\Delta\rho/\overline{\rho}=0.68$, and $\xi=16$ nm.

temporarily reorganized or better ordered the adsorbed surfactant layer on the treated mica. However, any rearrangement does not last long since subsequent approaches exhibited the same difficulty to transit from the second to the first oscillation. In the second experiment presented in Figs. 5(a) and 5(b) and analyzed in Figs. 9(c) and 9(d), the difficulty to expel the last layer of micelles was less pronounced since an inward jump was always measured at the equilibrium separation of $1.5a_0$. However, the modeling force cannot account correctly for the data at these small separations, as illustrated in Fig. 9. These observations suggest that the limit condition on the treated surface was certainly not fixed as supposed in the model for separations lower than 17 nm. On the other hand, this assumption seems quite robust for the larger separations. Indeed, beyond the second oscillation, up to large separations, no hysteresis was observed between compression and dilation runs. The corresponding measurements were highly reproducible and consistent between them. The fits were then performed exclusively over this range of separation. The fit parameters are reported in the Fig. 9 and in its caption. Note that the asymmetric ratio varies from one experiment to another. The analysis of the third experiment presented in Figs. 5(c) and 5(d) gives an intermediate value of $\Delta\rho/\overline{\rho}$. The scatter is meaningful in regard to the experimental accuracy, but its narrowness reflects the good homogeneity of the polymer coating. In the first experiment, we find also that the asymmetric ratio increases slightly on cooling, whereas in the second experiment the ratio can be maintained fixed without an affect on the fit accuracy. Of course, the smectic correlation length is found to increase as the lamellar transition is approached, but this information was already explicit in the evolution of the oscillation number. In

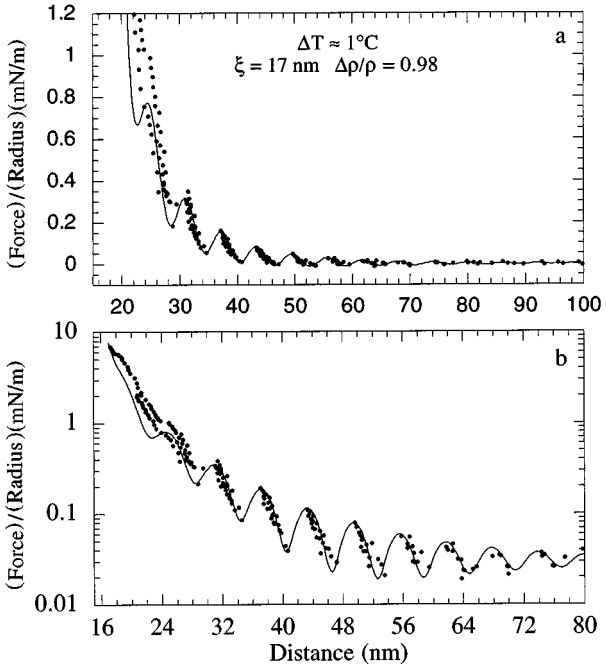

FIG. 10. Comparison between an experimental force profile and the modeling force (42) for two dissimilar surfaces. The solid symbols are the data measured between a bare mica and a mica coated with 44 000-MW poly-*l*-lysine immersed in a 38-wt. % CsPFO solution, while the line represents a fit using a prefactor $2\pi RL\overline{\rho}=7.6\times10^{-9}$ mN, an asymmetric ratio $\Delta\rho/\overline{\rho}=0.98$, and a correlation length $\xi=17$ nm.

the temperature range explored, ξ varies between 2 and 5 times the smectic layer thickness a_0.

In summary, the fit procedure shows that the modeling force can account for the experimental force profiles in spite of the restrictive assumption of fixed boundary conditions, which becomes questionable when only one or two layers are confined at the cell center. A similar conclusion comes from the analysis of the experiment when one of the two mica surfaces has been coated with the 44 000-MW polypeptide.

For instance, in Fig. 10, we present a numerical fit performed on the force profile displayed in Figs. 4(a) and 4(b). We found a large asymmetric ratio, meaning that the treated surface hardly induced the positional smectic order. The fitting curve is in good agreement with the data at large separations, beyond 30 nm, over the nine or ten oscillations recorded in this range, as the semilogarithmic plot in Fig. 10(b) illustrates it. Difficulty arises when only five presmectic layers or less remain between the surfaces at the cell center. In the corresponding separation range, the measurements recorded upon dilation do not reproduce those obtained upon compression as illustrated in Fig. 10. Moreover, the ultimate reminiscence of an oscillation is around 18 nm, corresponding approximately to the transition from three to two layers. At lower separations, the interaction is a stiff increasing monotonic repulsion. Accordingly, in order to carry out the fit procedure, we had to increase d_a of two layers, i.e., from a usual 3.8 to 16 nm, otherwise the prefactor of (42), $2\pi RL\overline{\rho}$, could not be kept consistent with the previous experiments. On the theoretical side, this feature means that the set of the two smectic layers next to the coated mica does not take part in the configuration changes imposed by the confinement. For the elastic response of the presmectic film, this surfactant layer is incompressible and for the order distribution this layer is frozen. From a physical point of view, this layer might correspond to an extension of the adsorbed surfactant layers. This supplementary adsorption might be due to a partial desorption of macromolecules resulting from the affinity competition between the negatively charged mica surface and the anionic surfactants. The corresponding free loops (or tails) of polymer are complexed by micelles, which are then trapped near the coated surface with a few numbers of degrees of freedom. This interpretation is not in agreement with the previous experiment at low concentration in the surfactant [i.e., 6%, Fig. 8(e)] since the observed depletion indicates that the squeezed micelles are not adsorbed on the surfaces. Therefore, if the partial desorption mechanism is real, it must arise at larger surfactant concentration. Another explanation could be that the enhanced roughness of the treated surface exhibits a coarseness large enough to restrict the freedom degrees of the closest micelles, greatly increasing their characteristic relaxation times. In other words, the coated surface exerts an ordering potential on the micelles with a finite range (i.e., two layers in the current experiment and corresponding to the characteristic length of its roughness) instead of a zero range, as assumed in the model. Although the SFA has provided valuable information about the real extent of the adsorbed layer not easily or directly obtainable by other techniques, this apparatus does not provide a complementary description at a microscopic level. Thus the interpretation of the previous observation without supplementary investigations can be only speculative.

Finally, we conclude with the reliability of the parameters determined from the analysis of the asymmetric experiments. Let us examine the set of the prefactor of (42), $2\pi RL\overline{\rho}$, obtained from the fits. According to the calculated asymmetric ratios, the prefactor would be quite constant since only $\overline{\rho}$ would vary of few percent from one experiment to another. Actually we found a rather large scatter for the prefactor $(5.5\pm2)\times10^{-9}$ mN. As we have already mentioned, the assumption of fixed boundary conditions, notably on the coated surface, is certainly too restrictive. A second difficulty is the correct determination of d_a, the extent of the surfactant layer near the treated mica that must be considered as frozen in the model (see the previous discussion). Finally, another limitation arises from the sensitivity of the device. Indeed, according to the theory, close to the transition $\Delta T/T\ll1$, the strength of the two contributions in the force (42) vanishes. The evolution of the elastic contribution is even more critical under strong asymmetry since the oscillation amplitudes are always weak [proportional to $(\rho_1\rho_2)^{1/2}$] whatever ΔT. Thus the SFA has been a powerful and accurate device in our study only for $\Delta T>1$ °C or when $\Delta\rho=0$ under symmetric conditions. Note that the prefactor $2\pi RL\overline{\rho}$ extracted from the fit presented in Fig. 2(b) for a symmetric case is 11×10^{-9} mN, which is in good agreement with the asymmetric mean value since a factor 2 is expected in $\overline{\rho}$ between the two conditions.

V. CONCLUSION

Previous studies on simple liquids consisting of isotropic [35] or anisotropic [36] molecules that have some tendency to align parallel to the surfaces have shown force profiles similar to the curves of Fig. 1. A small number of oscillations was obtained, giving the so-called solvation forces [19]. Oscillatory force profiles have also been measured in concentrated micellar solutions [32,37], where the oscillation periods have been found to fit with the aggregate diameters. Moreover, Horn, Israelachvili, and Perez have studied the interaction between two surfaces confining a droplet of a thermotropic nematic at fixed temperature [28]. From a not well understood long-range repulsion they observed the emergence of a structural interaction with up to six oscillations at short separations. More oscillations have been recorded in the force profiles of two surfaces immersed in a lyotropic regular lamellar phase [26,38,39]. The examples of oscillatory force profiles are numerous and rather varied in the literature. It is well established now that the oscillations often result from the elastic response of systems constrained by the confinement. A more difficult task is to discern other contributions in these oscillatory force profiles and their consequences. The present study provides an insight into such coupling since a second contribution has been clearly identified and we have been able to tune its behavior.

This second contribution arises from the distribution of the order between the two confining surfaces. It may be generalized to different natures of order and to the interactions between bodies when a preferential wetting occurs. However, it must be kept in mind that the results obtained both in the model and in the experimental situation depend on restrictions imposed at the boundaries. For instance, when the

boundary conditions are not fixed but evolve with the separation, the interaction between two dissimilar ordering surfaces (weak anchoring) may remain attractive whatever their separation, with a profile that will be of course different from that encountered when the two surfaces are similar. The assumption of a contact potential between the surfaces and the particles is also a very strong limitation. The introduction of a finite range would drastically change our present conclusion. As long as the potential range is lower than the order correlation length the current study is relevant, but in the other limit the net result would be completely different. The electrostatic double-layer repulsion is the best illustration.

[1] P. Sheng, Phys. Rev. Lett. **37**, 1059 (1976); Phys. Rev. A **26**, 1610 (1982).

[2] K. Miyano, Phys. Rev. Lett. **43**, 51 (1979).

[3] J. Als-Nielsen, F. Christensen, and P. S. Pershan, Phys. Rev. Lett. **48**, 1107 (1982).

[4] P. S. Pershan and J. Als-Nielsen, Phys. Rev. Lett. **52**, 759 (1984).

[5] B. M. Ocko, A. Braslau, P. S. Pershan, J. Als-Nielsen, and M. Deutsch, Phys. Rev. Lett. **57**, 94 (1986).

[6] Y. Shi, B. Cull, and S. Kumar, Phys. Rev. Lett. **71**, 2773 (1993).

[7] A. Poniewierski and T. J. Sluckin, Liq. Cryst. **2**, 281 (1987).

[8] S. Kralj, S. Žumer, and D. W. Allender, Phys. Rev. A **43**, 2943 (1991).

[9] D. W. Allender, G. P. Crawford, and J. W. Doane, Phys. Rev. Lett. **67**, 1442 (1991).

[10] G. S. Iannacchione and D. Finotello, Phys. Rev. Lett. **69**, 2094 (1992).

[11] A. Golemme, S. Žumer, D. W. Allender, and J. W. Doane, Phys. Rev. Lett. **61**, 2937 (1988).

[12] G. S. Iannacchione, G. P. Crawford, S. Zumer, J. W. Doane, and D. Finotello, Phys. Rev. Lett. **71**, 2595 (1993).

[13] N. A. Clark, T. Bellini, R. M. Malzbender, B. N. Thomas, A. G. Rappaport, C. D. Muzny, D. W. Schaefer, and L. Hrubesh, Phys. Rev. Lett. **71**, 3505 (1993).

[14] P. G. de Gennes, Langmuir **6**, 1448 (1990).

[15] L. Moreau, P. Richetti, and P. Barois, Phys. Rev. Lett. **73**, 3556 (1994).

[16] D. A. Antelmi, P. Kékicheff, and P. Richetti, J. Phys. (France) II **5**, 103 (1995).

[17] P. Petrov, U. Olsson, H. K. Christenson, S. Miklavic, and H. Wennerström, Langmuir **10**, 988 (1994).

[18] J. N. Israelachvili and G. E. Adams, J. Chem. Soc. Faraday Trans. I **74**, 975 (1978).

[19] J. N. Israelachvili, *Intermolecular and Surface Forces* (Academic, New York, 1985), and references therein.

[20] N. Boden, P. H. Jackson, K. McMullen, and M. C. Holmes, Chem. Phys. Lett. **65**, 476 (1979).

[21] N. Boden, S. A. Corne, M. C. Holmes, P. H. Jackson, D. Parker, and K. W. Jolley, J. Phys. (Paris) **47**, 2135 (1987).

[22] T. Afshar-Rad, A. I. Bailey, P. F. Luckham, W. Macnaughtan, and D. Chapman, Colloids Surf. **25**, 263 (1987).

[23] P. S. Pershan, J. Appl. Phys. **45**, 1590 (1974).

[24] P. S. Pershan and J. Prost, J. Appl. Phys. **46**, 2343 (1975).

[25] S. Marčelja and N. Radić, Chem. Phys. Lett. **42**, 129 (1976).

[26] P. Richetti, P. Kékicheff, and P. Barois, J. Phys. (France) II **5**, 1129 (1995).

[27] B. V. Derjaguin, Kolloid Z. **69**, 155 (1934).

[28] R. G. Horn, J. N. Israelachvili, and E. Perez, J. Phys. (Paris) **42**, 39 (1981).

[29] C. Rosenblatt, Phys. Rev. A **32**, 1115 (1985).

[30] T. Haven, D. Armitage, and A. Saupe, J. Chem. Phys. **75**, 352 (1981).

[31] V. Shubin, Langmuir **10**, 1093 (1994).

[32] P. Richetti and P. Kékicheff, Phys. Rev. Lett. **68**, 1951 (1992).

[33] P. F. Luckham and J. Klein, J. Chem. Soc. Faraday Trans. 1 **80**, 865 (1984).

[34] L. R. Dix, C. Toprakcioglu, and R. J. Davies, Colloids Surf. **31**, 147 (1988).

[35] R. G. Horn and J. N. Israelachvili, J. Chem. Phys. **75**, 1400 (1981).

[36] H. K. Christenson, D. W. R. Gruen, R. G. Horn, and J. N. Israelachvili, J. Chem. Phys. **87**, 1834 (1987).

[37] J. L. Parker, P. Richetti, P. Kékicheff, and S. Sarman, Phys. Rev. Lett. **68**, 1955 (1992).

[38] P. Kékicheff and H. K. Christenson, Phys. Rev. Lett. **63**, 2823 (1989).

[39] P. Richetti, P. Kékicheff, J. L. Parker, and B. W. Ninham, Nature **346**, 39 (1990).